Available online at www.sciencedirect.com
ScienceDirect
Nuclear Medicine and Biology 34 (2007) 55–70
NUCLEAR MEDICINE — AND — BIOLOGY
www.elsevier.com/locate/nucmedbio

# Evaluation of radiolabeled ML04, a putative irreversible inhibitor of epidermal growth factor receptor, as a bioprobe for PET imaging of EGFR-overexpressing tumors

Galith Abourbeh[a,b], Samar Dissoki[a], Orit Jacobson[a], Amir Litchi[a], Revital Ben Daniel[a], Desirediu Laki[a], Alexander Levitzki[b], Eyal Mishani[a,*]

[a]*Department of Medical Biophysics and Nuclear Medicine, Hadassah Hebrew University, Jerusalem 91120, Israel*
[b]*Unit of Cellular Signaling, Department of Biological Chemistry, The Alexander Silberman Institute of Life Sciences, The Hebrew University, Jerusalem 91904, Israel*

Received 24 October 2006; accepted 28 October 2006

**Abstract**

Overexpression of epidermal growth factor receptor (EGFR) has been implicated in tumor development and malignancy. Evaluating the degree of EGFR expression in tumors could aid in identifying patients for EGFR-targeted therapies and in monitoring treatment. Nevertheless, no currently available assay can reliably quantify receptor content in tumors. Radiolabeled inhibitors of EGFR-TK could be developed as bioprobes for positron emission tomography imaging. Such imaging agents would not only provide a noninvasive quantitative measurement of EGFR content in tumors but also serve as radionuclide carriers for targeted radiotherapy.

The potency, reversibility, selectivity and specific binding characteristics of ML04, an alleged irreversible inhibitor of EGFR, were established in vitro. The distribution of the F-18-labeled compound and the extent of EGFR-specific tumor uptake were evaluated in tumor-bearing mice.

ML04 demonstrated potent, irreversible and selective inhibition of EGFR, combined with specific binding to the receptor in intact cells. In vivo distribution of the radiolabeled compound revealed tumor/blood and tumor/muscle activity uptake ratios of about 7 and 5, respectively, 3 h following administration of a radiotracer. Nevertheless, only minor EGFR-specific uptake of the compound was detected in these studies, using either EGFR-negative tumors or blocking studies as controls.

To improve the in vivo performance of ML04, administration via prolonged intravenous infusion is proposed. Detailed pharmacokinetic characterization of this bioprobe could assist in the development of a kinetic model that would afford accurate measurement of EGFR content in tumors.


*Keywords:* ML04; TKS040; EGFR; Inhibitor; PET; Imaging

## 1. Introduction

Epidermal growth factor receptor (EGFR/c-ErbB1/HER1), along with HER2 (c-ErbB2/neu), HER3 (c-ErbB3) and HER4 (c-ErbB4), is a member of Subclass I of the receptor tyrosine kinase superfamily. The activation process of these receptors requires their homodimerization/heterodimerization, followed by juxtaposition of their cytoplasmic parts. This active conformation makes it possible for TK domains of the receptors both to bind ATP and to transphosphorylate each other. Receptor autophosphorylation on tyrosine residues both enhances the catalytic activity of kinases and provides docking sites for downstream signal transduction molecules that harbor SH2 or PTB domains. These interactions activate signal transduction pathways, which ultimately lead to multiple cellular processes, such as proliferation, differentiation, apoptosis, angiogenesis, cell adhesion and movement [1–7].

Aberrant family member signaling in tumors often involves EGFR and HER2 and is commonly caused by gene amplification, ligand overexpression (which causes persistent autocrine stimulation) or activating mutations [such as the $\Delta_{2-7}$ EGFR (EGFRvIII) mutation, which leads

* Corresponding author. Tel.: +972 2 6777931; fax: +972 2 6421203.
*E-mail address:* mishani@md.huji.ac.il (E. Mishani).

0969-8051/$ – see front matter © 2007 Elsevier Inc. All rights reserved.
doi:10.1016/j.nucmedbio.2006.10.012

to ligand-binding-independent constitutive activation] [8–10]. Overexpression of EGFR has been demonstrated in numerous human epithelial tumors, including cancers of the upper aerodigestive tract [non small cell lung cancer (NSCLC), small cell carcinoma of the head and neck, esophageal cancer and gastric cancer], as well as in gliomas and carcinomas of the colon, pancreas, breast, ovary, bladder and kidneys [8,11–13]. Furthermore, increasing evidence of a correlation between EGFR overexpression and metastasis formation, therapy resistance, poor prognosis and short survival gave impetus to the development of various anti-EGFR-targeted therapies. Examples of such therapies approved by the Food and Drug Administration include low-molecular-weight reversible EGFR TK inhibitors, such as gefitinib (Iressa, ZD1839; AstraZeneca, Wilmington, PA; for the treatment of locally advanced or metastatic chemotherapy-refractory NSCLC) and erlotinib (Tarceva; Genentech, San Francisco, CA; for the treatment of locally advanced or metastatic chemotherapy-refractory NSCLC), in combination with gemcitabine, the treatment of choice for locally advanced, inoperable or metastatic pancreatic cancer [14,15]. The chimeric anti-EGFR monoclonal antibody cetuximab (Erbitux; ImClone Systems, Inc.) has also been approved for the treatment of advanced metastatic colorectal cancer [16]. Additional anti-EGFR-targeted therapies, which are currently on clinical trial, include monoclonal antibodies, such as panitumumab (ABX-EGF) and ICR62, and low-molecular-weight compounds, such as the dual EGFR/HER2 inhibitor PKI-166 and the irreversible pan-erbB inhibitor CI-1033 [17,18].

The role that EGFR overexpression plays in cancer development is gradually unraveling. Responsiveness to either EGF stimulation or EGFR inhibition does not correlate well with EGFR overexpression, as shown in both cellular and in vivo studies, and the experience gained so far with clinical EGFR-targeted therapy trials indicates that the level of EGFR expression in tumors is, in itself, insufficient to account for their sensitivity to treatment [19–28]. It is important to evaluate the factors that might affect the success of anti-EGFR therapies. These include the phosphorylation status of EGFR in tumors, the role of EGFR in the molecular development and progression of both hormone-dependent and hormone-independent tumors, the dependence of tumor cells on EGFR for survival and the extent of EGFR blockade in tumors following anti-EGFR-targeted therapies.

Although EGFR content in tumors does not suffice to predict the success of treatments that aim to block this receptor, its overexpression in tumors is a prerequisite for the initiation of EGFR-targeted therapy. Thus, the ability to noninvasively determine EGFR content in tumors would aid in selecting patients who are likely to benefit from anti-EGFR-targeted therapy and, even more importantly, in monitoring such treatment. Furthermore, overexpression of EGFR in cancerous cells could be exploited as a "Trojan horse" for targeted therapies, regardless of tumors' dependence on signaling downstream of this receptor. Examples of such approaches include: (a) EGF bioconjugates with toxins, oligonucleotides or radionuclides, which induce cell death upon receptor-mediated endocytosis; (b) cytotoxic drug delivery via immunoliposomes that home to EGFR; and (c) EGFR TK inhibitors and anti-EGFR antibodies, which serve as radionuclide carriers for radiotherapy [29–36].

Imaging EGFR in tumors requires an adequate imaging modality, coupled to a suitable specific probe. Positron emission tomography (PET) is a noninvasive nuclear imaging modality, which allows in vivo quantitative spatial and temporal surveillance of radiolabeled molecular probes (tracers). Contrary to other prevalent imaging techniques such as computed tomography (CT) and magnetic resonance imaging, which mostly provide information on gross anatomy and functionality, PET imaging allows tracking of underlying cellular and biochemical events. To this end, either natural or synthetic molecules are labeled with positron-emitting isotopes such as $^{15}O$, $^{13}N$, $^{11}C$ and $^{18}F$, which have half-lives of approximately 2, 10, 20 and 110 min, respectively. Radiolabeled probes are subsequently introduced into subjects, after which their distribution is quantitatively monitored by PET imaging. In addition to the high intrinsic sensitivity and the unlimited tissue-depth penetration that characterize this technique, modern PET/CT scanners offer a more accurate anatomic localization of radioactivity, thereby promoting the interpretation of PET images and establishing this imaging methodology as the most suitable one for the in vivo molecular imaging of EGFR [35,37–43].

Previous reports relating to the radiosyntheses of labeled inhibitors and their biological evaluations in preclinical models indicated that reversible inhibitors of EGFR were inadequate for the imaging of tumors that overexpressed this receptor [37,42]. The competition between manifold higher levels of intracellular ATP and radioligands resulted in rapid washout of a labeled inhibitor from the tumor, making such compounds ineffective as PET reporter probes. Subsequently, attempts to develop irreversible inhibitors of EGFR as potential imaging agents have been made [41,43]. A recently published work has pointed out derivatives of the 4-dimethylamino-but-2-enoic acid [4-(phenylamino)-quinazoline-6-yl]-amide group due to their favorable profile [44]. These inhibitors, characterized by remarkable inhibitory potency toward EGFR, elevated chemical and biological stabilities, and sufficient selectivity with respect to other tyrosine kinase receptors, scored high as suitable candidates for the PET imaging of EGFR-overexpressing tumors. The current report describes the progress of our group in this field of research with one selected derivative, ML04 (also known as TKS040; Fig. 1). In vitro evaluation of parameters of interest, including inhibitory potencies in various cell lines, selectivity towards EGFR, specific binding measurements and interaction with the *mdr-1* gene product P-glycoprotein (P-gp), was followed by comprehensive biodistribution studies in nude mice using established xenograft models.

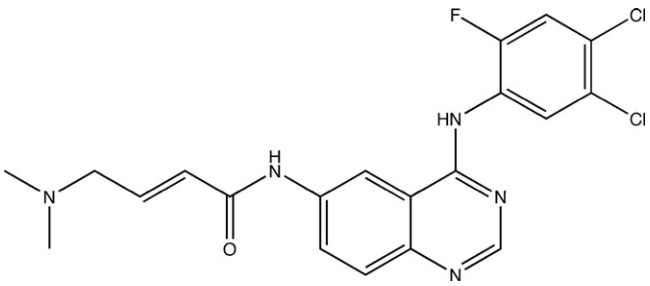

Fig. 1. ML04, a recognized irreversible inhibitor of EGFR tyrosine kinase.

The prospects of ML04 as a candidate tracer for the PET imaging of EGFR-overexpressing tumors are discussed.

## 2. Materials and methods

### 2.1. General

All chemicals were purchased from Sigma-Aldrich, Fisher Scientific, Merck or J.T. Baker. Chemicals—excluding tetrahydrofurane (THF), which was refluxed over sodium and benzophenone and freshly distilled prior to use—were used as supplied. Radiosyntheses were carried out on an F-18 module (GE, Munster, Germany), and specific radioactivities were determined by reverse-phase high-performance liquid chromatography (HPLC) columns (C-18 μBondapak Waters), using cold mass calibration curves. AG1478, a reversible specific inhibitor of EGFR, was synthesized according to a previously documented procedure [45].

### 2.2. Radiochemistry

[$^{18}$F]Fluoride ion was produced with an IBA cyclotron via an $^{18}$O(p,n)$^{18}$F nuclear reaction by irradiating 97% enriched [$^{18}$O]$H_2O$ with an 18-MeV proton beam. Radiosyntheses of [$^{18}$F]1,2-Dichloro-4-fluoro-5-nitro-benzene (**[$^{18}$F]1**) and [$^{18}$F]4,5-Dichloro-2-fluoro-aniline (**[$^{18}$F]2**) (Scheme 1) were performed in two commercial automated modules. The last four steps of [$^{18}$F]*N*-{4-[(4,5-dichloro-2-fluorophenyl)amino]quinazoline-6-yl}-dimethylamine-butynamide (**[$^{18}$F]ML04**) synthesis were performed with a homemade semiautomated system. Labeled compounds were analyzed with HPLC and compared to unlabeled standards as previously published [44].

#### 2.2.1. *[$^{18}$F]-1,2-Dichloro-4-fluoro-5-nitro-benzene [$^{18}$F]1*

An [$^{18}$O]$H_2O$/[$^{18}F^-$] (1930 mCi) mixture was trapped and transferred to a reactor through an ion exchange column (preactivated with 0.8 ml of EtOH and 3 ml of HPLC water) by elution with 0.5 ml of potassium carbonate (2.5 mg/0.5 ml). Following the addition of 1 ml of Kryptofix 222 solution (18 mg/ml $CH_3CN$), water was removed by azeotropic distillation with acetonitrile at 95°C under reduced pressure for 3 min. 1,2-Dichloro-4,5-dinitro-benzene (10 mg) dissolved in DMF (600 μl) was added, the reactor temperature was increased to 115°C and the reaction mixture was stirred for 20 min. After cooling the mixture to 30°C, 13 ml of water was added to the reactor, and the mixture was loaded on a C-18 cartridge (Waters Sep-Pak; preactivated with 5 ml of EtOH and 10 ml of sterile water). The product, **[$^{18}$F]1**, was eluted with 2 ml of EtOH into a collection vial after a total radiosynthesis time of 40 min and was obtained with an 80% radiochemical yield. The product was analyzed by a reverse-phase C-18 analytical column and eluted with 0.1 M acetate buffer (pH 3.8)/$CH_3CN$ (55%:45%) at flow=1 ml/min and rt=14.3 min.

#### 2.2.2. *[$^{18}$F]-4,5-Dichloro-2-fluoro-aniline [$^{18}$F]2*

Hydrazine monohydrate (200 μl) was added to a reactor containing 200 μl of EtOH/$H_2O$ (9:1) and Raney (Ra)–Ni (400 μl), and **[$^{18}$F]1** in EtOH/$H_2O$ was added dropwise to the reactor. Synthesis continued at 60°C for 7 min to yield **[$^{18}$F]2** with a 70% radiochemical yield. The product was diluted with 10 ml of water, passed through a C-18 cartridge and washed with water (5 ml), after which the column was dried under argon for 5 min. The product was eluted with i-PrOH (2.5 ml), analyzed on a reverse-phase C-18 analytical column and eluted with 0.1 M acetate buffer (pH 3.8)/$CH_3CN$ (55%:45%) at flow=1 ml/min and rt=11.66 min.

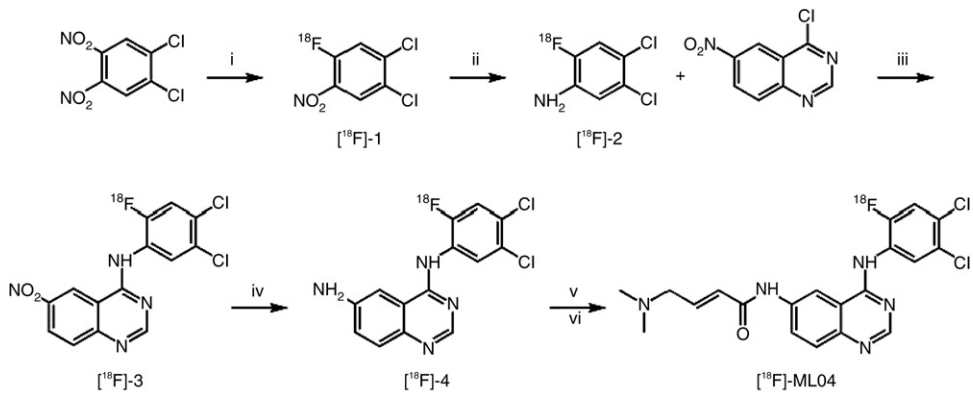

Scheme 1. Radiosynthesis of **[$^{18}$F]ML04**. (i) [$^{18}$F]KF, Kryptofix, DMF, 115°C, 20 min. (ii) $H_2NNH_2 \cdot H_2O$, Ra–Ni, EtOH/$H_2O$ (9:1), 60°C, 7 min. (iii) i-PrOH, 100–105°C, 20 min. (iv) $H_2NNH_2 \cdot H_2O$, Ra–Ni, EtOH/$H_2O$ (9:1), 65°C, 10 min. (v) Br/Cl-crotonylchloride, *N*,*N*-DIPEA, THF, 0°C, 20 min. (vi) Dimethylamine in THF (2 M), 0°C, 15 min.

*2.2.3. [$^{18}$F](4,5-Dichloro-2-fluoro-phenyl)-(6-nitro-quinazoline-4-yl)-amine ([$^{18}$F]3)*

4-Chloro-6-nitro-quinazoline (20 mg), dissolved in i-PrOH (0.5 ml), was added to a solution of **[$^{18}$F]2** in i-PrOH (2.5 ml). The reaction mixture was refluxed at 100–105°C for 5 min, and a second batch of 4-chloro-6-nitro-quinazoline (20 mg) was added. The reaction mixture was refluxed for an additional 15 min to obtain **[$^{18}$F]3** with an 80% radiochemical yield. The product was analyzed on a reverse-phase analytical column and eluted with 0.1 M acetate buffer (pH 3.8)/$CH_3CN$ (55%:45%) at flow=1 ml/min and rt=20.92 min.

*2.2.4. [$^{18}$F]N$^4$-(4,5-Dichloro-2-fluoro-phenyl)-quinazoline-4,6-diamine ([$^{18}$F]4)*

The vial containing **[$^{18}$F]3** was transferred to another heating bath (65°C), and EtOH/$H_2O$ (9:1; 250 μl), hydrazine monohydrate (450 μl) and Ra–Ni (400 μl) were added. The reaction mixture was stirred and heated to 65°C for 10 min to obtain **[$^{18}$F]4** with a 70% radiochemical yield. The solution was cooled, diluted with water (10 ml) and loaded onto C-18 Sep-Pak, and the column was dried under argon for 10 min for the next step. The product was analyzed on a reverse-phase analytical column and eluted with 0.1 M acetate buffer (pH 3.8)/$CH_3CN$ (55%:45%) at flow=1 ml/min and rt=9.73 min.

*2.2.5. [$^{18}$F]-N-{4-[(4,5-dichloro-2-fluorophenyl)amino] quinazoline-6-yl}-dimethylamine-butynamide ([$^{18}$F]-ML04)*

**[$^{18}$F]4** was eluted with dry THF (2.5 ml) into a conical vial at 0°C, followed by the addition of *N*,*N*-diisopropylethylamine into THF (20 μl/ml, 250 μl) and Br/Cl-crotonyl-chloride in THF (100 mg/ml, 0.8 ml). The reaction mixture was stirred for 20 min at 0°C and was used for the next step without any further treatment. The product was analyzed by a C-18 analytical column under the same conditions (rt=21.5 and 23.8 min on the first peak and on the second peak, respectively). Dimethylamine (2 M) in THF (1 ml) was added to the solution at 0°C, and the reaction continued for 15 min. The solution was evaporated under argon atmosphere to a volume of 700 μl, followed by the addition of $CH_3CN/H_2O$ (1:1). The product was analyzed on a reverse-phase C-18 column (rt=11.3 min) and purified using an HPLC reverse-phase C-18 preparative column, generating **[$^{18}$F]ML04** at an overall average of 14% radiochemical yield, a specific activity of 1800 Ci/mmol and a 98% radiochemical purity ($n$=10). HPLC conditions were as follows: C-18 preparative column and 0.1 M ammonium formate/$CH_3CN$ (53%:47%) at flow=5 ml/min and rt=35 min.

*2.3. Cell culture*

The human glioma cell line U87MG, which expresses a moderate amount of wild-type EGFR, and its subline U87MG.wt EGFR, which overexpresses wild-type EGFR, were described previously [46]. These, as well as the EGFR-negative U138MG human glioma cell line and the EGFR-overexpressing MDA-MB-468 human breast adenocarcinoma cell line, were grown in Dulbecco's modified Eagle's medium (DMEM; Biological Industries, Kibbutz Beit Ha'Emek, Israel) supplemented with 10% fetal calf serum (FCS) and antibiotics ($10^5$ U/L penicillin and 100 mg/L streptomycin) at 37°C in 5% $CO_2$. Similar growth conditions were maintained for the squamous cell lung carcinoma cell line PC10 and for the human NSCLC cell line NCI-H1975, except for the replacement of DMEM with RPMI 1640 (Biological Industries). NCI-H1975 cells were also supplemented with Hepes buffer (10 mM) and sodium pyruvate (1 mM). Lastly, porcine aortic endothelial PAE/KDR cells, which express VEGFR-2, were cultured in Ham's F12 medium (Biological Industries), supplemented with 10% FCS and antibiotics.

*2.4. Irreversibility test protocol*

Inhibitory potency and the extent of irreversible inhibition that ML04 exerts on the phosphorylation of EGFR were evaluated in A431 vulval carcinoma, MDA-MB-468 breast carcinoma, PC10 lung carcinoma and NCI-H1975 NSCLC cells, as previously described [41]. Briefly, A431 ($1\times10^5$ cells/well), MDA-MB-468 ($3\times10^5$ cells/well), PC10 ($1\times10^5$ cells/well) or NCI-H1975 cells ($1.5\times10^5$ cells/well) were grown in six-well plates for 48 h and further maintained in a serum-free medium for an additional 18 h. Duplicate sets of cells were incubated with ML04 at various concentrations (0.05% DMSO, 0.1% EtOH) for 1 h, after which the inhibitor was removed and a serum-free medium was added to the wells. One set of cells was stimulated with EGF immediately after removal of the inhibitor, while the other set of cells underwent EGF stimulation only 8 h after removal of the inhibitor from the medium and successive rinsing with phosphate-buffered saline (PBS). Cell lysates were prepared and loaded onto sodium dodecyl sulfate–polyacrylamide gel electrophoresis (8% acrylamide) for Western blot analysis, and the extent of EGFR phosphorylation was evaluated by measuring the signal intensity of the corresponding phosphotyrosine band using a mix of antiphosphotyrosine antibodies PY20 (Santa Cruz Biotechnology, Inc.) and 4G10 (produced from Su4G10 hybridoma cells). For each cell line, three independent assays were performed. Each assay was performed in duplicate.

*2.5. c-Src and IGF-1 receptor kinase assays: enzyme-linked immunosorbent assay (ELISA)*

Purification of GST-Src from *Escherichia coli* and purification of IGF-1 receptor from mouse embryo fibroblasts have been described, and kinase activities have been assessed by ELISA according to a previously published method [47,48]. In brief, the general tyrosine kinase substrate poly(Glu-Tyr) (4:1; Sigma) was coated onto 96-well Maxisorp plates (Nunc). Purified GST-Src (50 ng/well) was incubated in 20 mM Tris·HCl (pH 7.4) and 10 mM $MgCl_2$ containing ML04 at increasing

concentrations (0.5% DMSO) for 20 min at 37°C. Alternatively, semipurified IGF-1 receptor (10 ng/well) was incubated in 20 mM Tris·HCl (pH 7.4), 10 mM $MgCl_2$ and 5 mM $MnAc_2$ containing ML04 at increasing concentrations for 20 min at 30°C. Phosphorylation of tyrosyl residues was initiated by the addition of 20 μM ATP and was terminated 10 min later by the addition of an ethylenediamine tetraacetic acid (EDTA) solution (pH 8.0) to a final concentration of 200 mM. The plates were washed with TBST buffer [10 mM Tris·HCl (pH 7.4), 0.2% Tween-20 and 170 mM NaCl], blocked with 5% low-fat milk in TBST and incubated with the monoclonal antiphosphotyrosine-peroxidase-conjugated antibody PT-66 (Sigma) for 45 min at room temperature. Detection was carried out using a color reagent, 2,2′-azido-bis 3-ethyl-benzthiazoline-6-sulfonic acid (ABTS) (Sigma), in citrate phosphate buffer (pH 4.0) containing 0.004% $H_2O_2$. The optical density at 405 nm was measured, and $IC_{50}$ values were calculated using the Regression program (Blackwell Scientific Software; Onsey Mead, Oxford, UK) based on three independent assays, each with duplicate samples.

### 2.6. Inhibition of VEGFR-2 phosphorylation in PAE/KDR cells

Subconfluent PAE/KDR cells were starved overnight in a serum-free medium containing 0.01 mg/ml bovine serum albumin and were incubated with ML04 at increasing concentrations (0.05% DMSO, 0.1% EtOH) for 1 h. Cells were incubated with $Na_3VO_4$ (100 μM, 5 min) to inhibit phosphatase activity and were stimulated for 5 min at 37°C with 50 ng/ml VEGF-$A_{165}$ (CytoLab Ltd., Israel). Following a wash with ice-cold PBS containing 100 μM $Na_3VO_4$, cell lysates were prepared in boiling Laemmli buffer. The extent of VEGFR-2 phosphorylation was evaluated by Western blot analysis, as described in Section 2.4. The assay was repeated twice, using duplicate samples.

### 2.7. Interaction of ML04 with the mdr-1 gene product P-gp

The CEM wild-type human lymphoblastoid cell line and the multidrug-resistant CEM Col1000 cell line were generous gifts from Dr. W.D. Stein (The Hebrew University of Jerusalem, Jerusalem, Israel) and have been previously described [49]. Cell lines were grown in suspension in a 5% $CO_2$ atmosphere at 37°C using RPMI 1640 medium supplemented with 10% FCS and antibiotics. The multidrug-resistant cell line CEM Col1000 was also supplemented with 1 μg/ml colchicine (Sigma).

#### 2.7.1. Inhibition of P-gp-dependent efflux of calcein AM from cells

Cell suspensions (100 μl, $2\times10^6$ cells/ml in PBS containing 10 mM glucose) were incubated for 10 min at 37°C in 96-well Maxisorp plates (Nunc) in the presence of either ML04 or verapamil (Teva Pharmaceutical Industries Ltd., Israel), an established P-gp modulator [50,51]. Stock concentrations of ML04 were prepared in DMSO to achieve a final DMSO concentration of 0.5%. The reaction was initiated by the addition of 20 μl of calcein AM (Molecular Probes, The Netherlands) to reach a final concentration of 500 nM. Fluorescence was recorded from the bottom of the wells every 60 s for 90 min, with excitation of 485 nm and emission of 530 nm, at a temperature of 37°C, using a microplate fluorescence reader (FLUOstar; MTX Lab Systems, Inc.). The initial rate of fluorescence increase in the interval from 0 to 900 s was used to evaluate the degree of P-gp inhibition, based on a previously described method [49].

#### 2.7.2. Modulation of [$^{11}$C]ML04 cellular uptake by verapamil

The radiosynthesis of [$^{11}$C]ML04 has been described [41]. CEM cells were suspended in PBS containing 10 mM glucose ($2\times10^6$ cells/ml), divided into glass tubes ($2\times10^6$ cells/tube), and incubated for 5 min at 37°C with shaking. Increasing concentrations of verapamil (diluted in PBS containing 10 mM glucose) were added to the cells in a volume of 800 μl, 10 min prior to the addition of the tracer. [$^{11}$C]ML04 (104–151 mCi/μmol at the time of addition; final concentration, 0.15% EtOH) was spiked into the tubes in a 200-μl volume and was further incubated with cells for 1 h with gentle shaking. Cells were harvested with a cell harvester (Brandel, Inc.) and washed thrice with PBS, and cell-associated activity was measured by exposing oven-dried filters (Brandel, Inc.; GF/B grade, preincubated in 0.3% polyethyleneimine for 3 days at 4°C) to a phosphor imager plate (BAS-IP MS 2040; Fuji Photo Film Co., Ltd.). The plates were scanned with an Image Reader Bas-1000 V1.8 scanner, and measurements were made with TINA 2.10 g software. The assay was repeated four times, with similar results.

ML04 was evaluated as a substrate for the P-gp efflux pump using two expressions from the literature [50]:

$$\underset{(FR)}{\text{Fold reversal}} = \frac{\text{Maximal } [^{11}\text{C}]\text{ ML04 uptake in CEM Col1000 cells in the } \textit{presence} \text{ of verapamil}}{[^{11}\text{C}]\text{ ML04 uptake in CEM Col1000 cells in the } \textit{absence} \text{ of verapamil}}$$

$$\underset{(RRF)}{\text{Residual resistance factor}} = \frac{[^{11}\text{C}]\text{ ML04 uptake in CEM wild type cells}}{\text{Maximal } [^{11}\text{C}]\text{ML04 uptake in CEM Col1000 cells.}}$$

### 2.8. Specific binding studies of [$^{18}$F]ML04 in intact A431 cells

A431 cells were suspended in PBS ($5\times10^5$ cells/ml), divided into aliquots of $1\times10^6$ cells/tube and incubated at 4°C for 30 min with gentle shaking. To measure nonspecific binding (NSB), one set of tubes was incubated with the reversible EGFR TK inhibitor AG1478 (5 μM, 0.1% DMSO, 30 min). To measure total binding, a parallel set of tubes was incubated with 0.1% DMSO vehicle. **[$^{18}$F]ML04** (30–100 mCi/μmol; final concentration, 0.125% EtOH) was then added to the tubes at various concentrations (2.5–75 nM) for 45 min. Both NSB and total binding measurements were carried out using duplicate

samples. For each concentration of **[$^{18}$F]ML04** that was added to the cells, a corresponding control sample, consisting of cell-free PBS, was incubated with the same concentration of the labeled inhibitor so as to calculate the cell-independent retention of activity by filters. Following incubation with the labeled inhibitor, the cells were harvested with a cell harvester (Brandel, Inc.), and the tubes were washed three to five times with PBS. Filters (Brandel, Inc.; GF/B grade, preincubated in 0.3% polyethyleneimine for 3 days at 4°C) were dried and exposed to a phosphor imager plate (BAS-IP MS 2040; Fuji Photo Film Co., Ltd.). The plates were scanned with an Image Reader Bas-1000 V1.8 scanner, and measurements were made with TINA 2.10 g software. Signal intensities obtained for both sets of measurements were corrected for the cell-independent filter retention of activity by deducting the signals of control samples (PBS only). Specific binding was calculated by subtracting the NSB signal from the corresponding total binding signal at each concentration of ML04, and data analysis was performed with GraphPad Prism, version 2.01 (GraphPad Software, Inc.). $B_{max}$ value was determined empirically by converting signal intensities (in pixels) obtained by a phosphor imager plate to inhibitor concentrations, using a calibration curve.

### 2.9. Animal studies

NUDE-Hsd athymic nude nu mice (6–8 weeks) weighing ~25 g were obtained from Harlan Industries, Inc. All animal studies were conducted under a protocol approved by the Research Animal Ethics Committee of The Hebrew University of Jerusalem and in accordance with its guidelines. Mice were allowed to acclimate in the animal facility for at least a week prior to their inoculation with tumor cells. They were routinely kept in 12-h light/dark cycles and provided with food and water ad libitum.

### 2.10. Xenograft models of human glioma U87MG.wt EGFR and U138MG tumors

Human glioma U87MG.wt EGFR and U138MG cells were cultured in vitro as above, and subconfluent cultures were released from flasks with trypsin, counted with a hemocytometer using trypan blue and suspended in sterile PBS at a volume of $1.5\times10^7$ and $2.0\times10^7$ ml$^{-1}$, respectively. Cell suspensions were supplemented with Matrigel (20% vol/vol; BD Biosciences, Beit-Ha'Emek, Israel) and thoroughly mixed prior to their injection into mice. Mice were anesthetized by intraperitoneal administration of a mixture of ketamine (140 mg/kg) and xylazine (15 mg/kg) and inoculated subcutaneously with either $1.5\times10^6$ U87MG.wt EGFR cells or $2.0\times10^6$ U138MG cells. Due to the different growth rates of the tumors, U87MG.wt EGFR cells were inoculated about 10 days before U138MG cells were inoculated. On the day of biodistribution studies, therefore, the average age of the U87MG.wt EGFR and U138MG tumors was 21 and 11 days, respectively.

### 2.11. Histology and immunohistochemistry

Histological and immunohistochemical validation of tumor models was performed by Patho-Lab Ltd. (Rehovot, Israel) prior to biodistribution studies. U87MG.wt EGFR ($n=7$) and U138MG ($n=7$) tumors were generated as described above. Tumor specimens of 26 days (U87MG.wt EGFR) and 14 days (U138MG) were fixed in 4% formalin and delivered to Patho-Lab Ltd. for further treatment. Briefly, tumor samples were paraffin-embedded, serial paraffin sections of the tumors were deparaffinized and rehydrated, and endogenous peroxidase activity was quenched by immersing the sections in 3% $H_2O_2$ for 10 min, followed by proteolytic digestion with 0.1% pronase and microwave heating of tumor sections in citrate buffer (pH 6.0) for 10 min. The tumor sections were incubated with primary antibodies specific for human wild-type EGFR (clone 31G7, diluted 1:100; Zymed Laboratories, South San Francisco, CA) and Factor VIII (rabbit anti-Factor-VIII-related antigen; Zymed Laboratories). The sections were immunohistostained with the Histomouse-Max Kit (Zymed Laboratories) using AEC as chromogen (*N*-Histofine Simple Stain AEC Solution; Nichirei Corporation, Tokyo, Japan). Negative control staining was carried out by omitting primary antibodies. Finally, tissue sections were counterstained with Mayer's hematoxylin and coverslipped.

### 2.12. [$^{18}$F]ML04 biodistribution studies in tumor-bearing mice

Biodistribution studies were carried out with NUDE-Hsd athymic nude nu mice (10–17 weeks) bearing U87MG.wt EGFR tumors 19–25 days old and/or U138MG tumors 9–14 days old. In the first set of studies, **[$^{18}$F]ML04** was injected into the animals using Intralipid 10% (Hadassah

Table 1
Inhibitory potencies of ML04 toward EGFR and related tyrosine kinases in cell-free assays and intact cells

| Investigated tyrosine kinase (cell line) | $IC_{50}$ values in intact cells (nM)[a] | | $IC_{50}$ values in a cell-free kinase assay (nM)[a] |
|---|---|---|---|
| | Immediately after removal of the inhibitor | 8 h after removal of the inhibitor | |
| EGFR (A431) | 4–10[b] | 10–50[b] | 0.11±0.08[b] |
| EGFR (MDA-MB-468) | 1–5 | 1–5 | |
| EGFR (PC10) | 10–50 | 10–50 | |
| EGFR (NCI-H1975) | 25 | ND | |
| EGFR (DHER14) | 4[b] | ND | |
| HER2 (CSH12) | 25–50[b] | ND | ND |
| PDGFR (NIHPDGFR) | >1000[b] | ND | ND |
| VEGFR-2 (PAE/KDR) | >10,000 | ND | ND |
| c-Src | ND | | 118±26 |
| IGF-1 receptor | ND | | >15,000 |

ND, not determined.

[a] Median inhibitory concentrations ($IC_{50}$) were obtained from at least three independent experiments. Where applicable, results are presented as mean±S.D.

[b] Studies investigating the inhibitory potency toward the EGFR and related tyrosine kinases were carried out using either intact cells or a cell-free kinase assay, as previously described [44].

Hospital, Jerusalem, Israel) as vehicle. To this end, **[$^{18}$F]ML04** was dissolved in EtOH and added to the emulsion at a 10% (vol/vol) ratio, followed by evaporation of EtOH at 50°C under gentle nitrogen flow for 10 min. In subsequent studies, **[$^{18}$F]ML04** was injected in a 5–10% EtOH/saline solution as vehicle.

For blocking studies, unlabeled ML04 was dissolved in Intralipid 10% and injected intravenously at a dose of 5–8 mg/kg, 1 h prior to tracer injection.

**[$^{18}$F]ML04** (45±28 μCi, 257±99 mCi/μmol, 100–250 μl) was injected via the lateral tail vein. At allotted time points, blood was drawn from the orbital sinus, mice were sacrificed by cervical dislocation and selected organs were excised, weighed and measured for their radioactive content using a γ-counter (1480 Wizard 3″). Distribution of activity was calculated as the percentage of injected dose per gram of organ (% ID/g). Activity uptake ratios of various organs were calculated by dividing the corresponding calculated percentages of injected dose per gram of organ.

### 2.13. Statistical analysis

Results are presented as mean±S.E.M., unless otherwise stated. All statistical analyses compared both the percentages of injected dose per gram of organ and the tumor/tissue activity uptake ratios of corresponding studies. Both the comparison of vehicles and the effect of blocking were evaluated using paired *t* test, and the level of significance was set at $P<.05$.

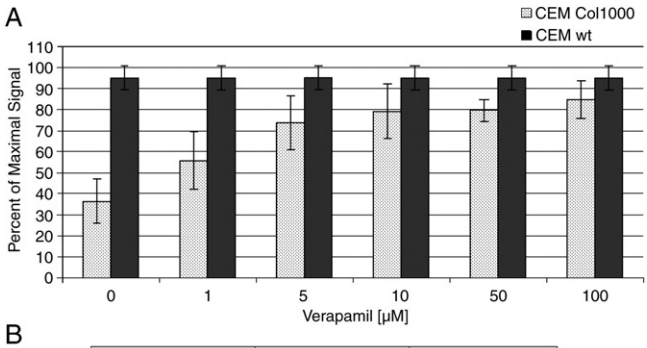


| Study No. | FR* | RRF** |
|---|---|---|
| 1 | 2.2 | 1.2 |
| 2 | 2.9 | 1.2 |
| 3 | 2.5 | 1.2 |
| 4 | 2.7 | 1.3 |
| Mean ± SD | 2.6 ± 0.3 | 1.2 ± 0.1 |

$$^{*}\text{Fold Reversal (FR)} = \frac{\text{Maximal } [^{11}\text{C}]\text{-ML04 uptake in CEM Col1000 cells in the } \textit{presence} \text{ of verapamil}}{[^{11}\text{C}]\text{-ML04 uptake in CEM Col1000 cells in the } \textit{absence} \text{ of verapamil}}$$

$$^{**}\text{Residual Resistance Factor (RRF)} = \frac{[^{11}\text{C}]\text{-ML04 uptake in CEM wt cells}}{\text{Maximal } [^{11}\text{C}]\text{-ML04 uptake in CEM Col1000 cells}}$$

Fig. 2. ML04 is a substrate for the ATP-dependent efflux transporter P-gp. Carbon-11-labeled ML04 was incubated with either P-gp-expressing CEM Col1000 cells or control CEM wild-type cells in the presence of increasing concentrations of verapamil, a modulator of the transporter. Cells were harvested, and their radioactive content was measured with a phosphor imager plate. (A) Cellular uptake of [$^{11}$C]ML04 into CEM Col1000 cells is enhanced as verapamil concentration is increased (mean±S.D.; $n=4$). (B) [$^{11}$C]ML04 uptake in CEM Col1000 cells after the reversal of the efflux activity of P-gp is on par with uptake in CEM wild-type cells.

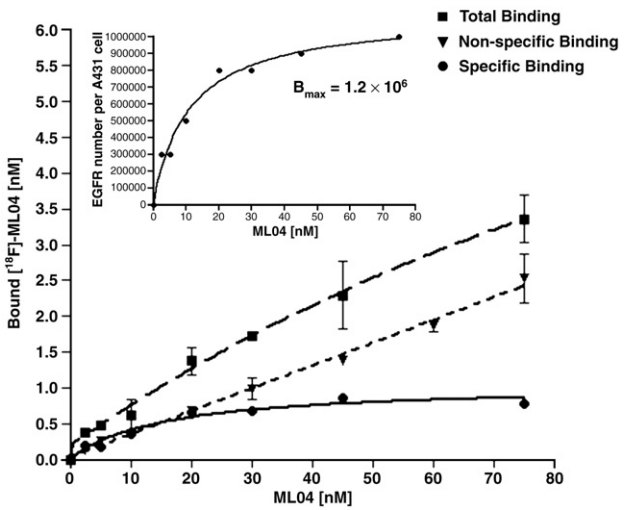


Fig. 3. Fluorine-18-labeled ML04 accurately measures EGFR content in cells. **[$^{18}$F]ML04** was incubated with A431 cells either in the presence or in the absence of AG1478, an EGFR-specific inhibitor, signifying NSB and total binding, respectively. Cells were harvested, washed to remove unbound tracer and exposed to a phosphor imager plate for measurement of radioactive signal. Specific binding at each inhibitor concentration was calculated by subtracting the NSB signal from the corresponding total binding signal. Calculation of EGFR content per cell, as obtained in one demonstrative experiment, is illustrated in the insert, yielding a $B_{max}$ value of $1.2\times10^6$ receptors/A431 cell. The average number of receptors per cell, from four experiments, was $(1.56\pm0.36)\times10^6$.

## 3. Results

### 3.1. Radiosynthesis of *[$^{18}$F]ML04*

The previously described radiosynthesis of **[$^{18}$F]ML04** is depicted in Scheme 1 [52]. 1,2-Dichloro-4,5-dinitro-benzene was reacted with a solution of [$^{18}$F]KF and Kryptofix in DMF at 115°C for 20 min to obtain **[$^{18}$F]1** with an 80% radiochemical yield. Reaction of the latter with hydrazine monohydrate and Ra–Ni at 60°C for 7 min yielded **[$^{18}$F]2** with a 70% radiochemical yield. 4-Chloro-6-nitro-quinazoline and **[$^{18}$F]2** were coupled in i-PrOH at 100°C to yield **[$^{18}$F]3** with an 80% radiochemical yield. Product **[$^{18}$F]3** was reacted with hydrazine monohydrate and Ra–Ni at 65°C to obtain the reduced **[$^{18}$F]4** with a 70% radiochemical yield. Reaction of the latter with Br/Cl-crotonylchloride and diisopropylethyl amine at 0°C, followed by reaction with dimethylamine, provided **[$^{18}$F]ML04**, with an overall decay-corrected radiochemical yield of 14%, radiochemical purity of 98%, average specific activity of 1800 Ci/mmol ($n=10$) and total radiosynthesis time of 4 h, including purification and formulation.

### 3.2. ML04 is a potent selective irreversible inhibitor of EGFR

Irreversible inhibition of EGFR by ML04 has been previously illustrated in human epidermoid A431 cells,

Table 2
Validation of human glioma xenografts in nude mice, by histopathology and immunohistochemistry[a]

| Tumor model | Weight (mg) | Necrosis (%)[b] | Mitosis per high-power field | Inflammation | Vessels per high-power field[c] | EGFR staining |
|---|---|---|---|---|---|---|
| U87MG.wt EGFR ($n=7$) | 269±113 | 7±9 | 4.0±1.1 | None present | 8.4±1.5 | Positive (>80%) |
| U138MG ($n=7$) | 221±94 | 23±8 | 2.6±1.0 | Mild leukocytic infiltration | 4.9±1.7 | Negative |

[a] Results are presented as mean±S.D.
[b] The percentage of necrosis is approximate, encompassing necrotic areas as well as nontumor areas, such as foci of acellular homogenous protein-like materials.
[c] Vessels per high-power field were assessed by staining for Factor VIII. The vessels were counted in viable tumor areas, as well as in areas of proteinaceous materials. Stained vessels were identified by their endothelial lining and by the presence of at least one red blood cell in their lumen.

which overexpress this receptor. The extent to which ML04 inhibits the phosphorylation of EGFR was further validated using three additional human cell lines that express this receptor: PC10 lung carcinoma, MDA-MB-468 breast carcinoma and NCI-H1975 NSCLC cells. As indicated in Table 1, remarkable inhibitory potency of ML04 was demonstrated in various cell lines, with $IC_{50}$ values ranging from 1 to 50 nM. Similar $IC_{50}$ values obtained both immediately after and 8 h after removal of the inhibitor from the medium suggest that ML04 binds EGFR covalently and inhibits receptor activation in an irreversible manner. Fry et al. [53] have originally introduced this cell-based assay as an additional supporting indicator of irreversible bonding. Since their pioneering work, this methodology has gained recognition from the research community as a reliable criterion of irreversible inhibition and has been employed by various groups [44,54,55].

Selectivity to EGFR, vis-à-vis other closely related tyrosine kinases, was tested in either cell-free or cellular assays. Comparison of apparent $IC_{50}$ values (Table 1) in each assay category revealed at least a 250-fold higher inhibitory potency toward EGFR compared to other tyrosine kinases, with the exception of HER2. The $IC_{50}$ towards EGFR was only one order of magnitude lower than the $IC_{50}$ towards HER2, which shares an 80% homology with EGFR in its kinase domain.

### *3.3. ML04 is a substrate for the ATP-dependent efflux pump P-gp*

Two assays were carried out to study the nature of the interaction between P-gp and ML04. The ability of ML04 to modulate the ATP-dependent efflux of this transporter was tested using calcein AM, a nonfluorescent dye that diffuses through the cell membrane and is a substrate for the efflux pump P-gp, which carries it out of the cell. Within the cell, cytoplasmic esterases release fluorescent calcein from calcein AM molecules that have escaped P-gp carriers. Thus, inhibition of P-gp activity results in intracellular accumulation of fluorescent calcein, and the kinetics of calcein accumulation reflects the extent of P-gp inhibition by various substances [49].

ML04 (0–500 μM) or verapamil (0–200 μM), an established modulator of P-gp, was incubated with CEM Col1000 cells, which express this transporter, followed by addition of calcein AM and continuous monitoring of fluorescence. Maximal inhibition of P-gp was attained at an ML04 concentration of ~125 μM and was about 50% of the maximal inhibition obtained with 200 μM verapamil (data not shown). Further inhibition of the efflux activity of P-gp could not be obtained by increasing the concentration of ML04.

The second study addressed the possibility that ML04 is extruded by P-gp. CEM wild-type or CEM Col1000 cells

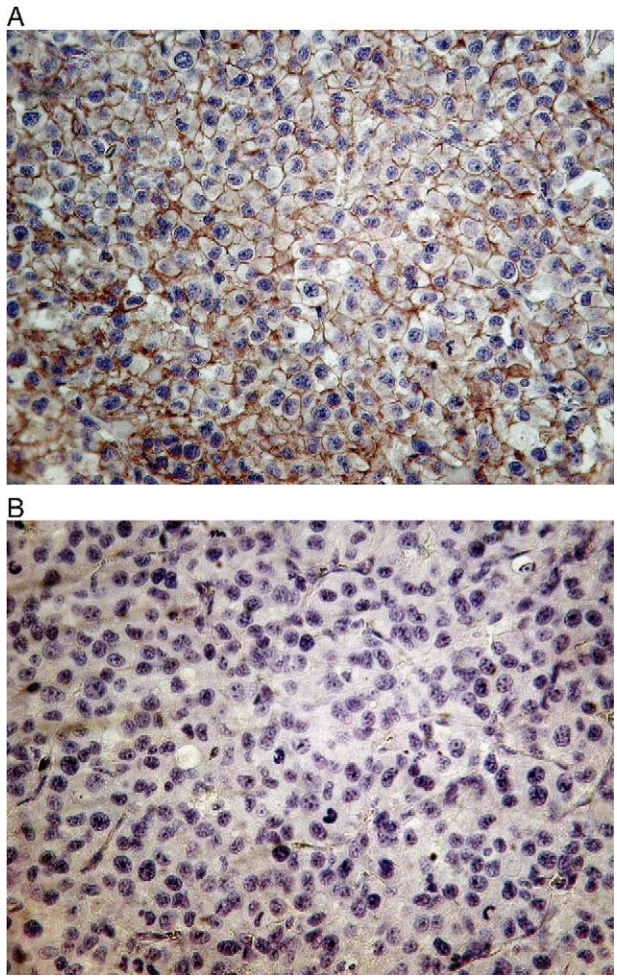


Fig. 4. Immunohistochemical staining of human glioma xenografts confirms that EGFR overexpression is confined to U87MG.wt EGFR tumors. U87MG.wt EGFR (A) and U138MG (B) tumor models of 26 and 14 days, respectively, were generated as described under Materials and Methods. Deparaffinized sections were stained for the expression of human EGFR, followed by counterstaining with Mayer's hematoxylin for assessment of viability and proliferation.

were treated with increasing concentrations of verapamil and were spiked with [$^{11}$C]ML04 [41]. Following 1 h of incubation with the tracer, cells were harvested and cell-associated radioactivity was measured with a phosphor imager plate. Fig. 2A summarizes the results of this assay, demonstrating increased cellular uptake of the C11-labeled compound with increased concentration of verapamil. Enhancement of the cellular uptake of [$^{11}$C]ML04 due to the inhibition of P-gp was evaluated with the two formulas presented in Fig. 2B [50]. As indicated, a twofold to a threefold increase in the cellular uptake of the tracer was achieved when P-gp was inhibited, approaching the maximal uptake in CEM wild-type cells.

### 3.4. ML04 is capable of accurately measuring EGFR content in intact cells

As a candidate bioprobe for tracking changes in the content of EGFR in tumors, ML04 must offer accurate measurement of receptor levels, with adequate levels of specific binding. These parameters were evaluated in binding studies, employing F-18-labeled ML04 and A431 cells, which contain approximately $1\times10^6$ to $2\times10^6$ EGFR molecules/cell [56–58]. Briefly, $1\times10^6$ cells were spiked with the labeled inhibitor in the presence or in the absence of an excess of the nonradioactive EGFR-specific inhibitor AG1478, representing NSB and total binding, respectively. After incubation with the radiotracer, the cells were harvested and total radioactivity within the cells was measured. Calculation of the number of EGFRs per cell ($B_{max}$) was performed by subtracting NSB values from total binding values at each concentration of ML04, as illustrated in Fig. 3. ML04 was capable of accurately measuring the cellular content of EGFRs, yielding an average value of $(1.56\pm0.36)\times10^6$ receptors/cell ($n=4$). An average maximal specific binding of 72±6% of total binding was attained at an ML04 concentration approaching EGFR concentration in the assay. However, as indicated by the graphic presentation in Fig. 3, high levels of NSB were perceived at higher inhibitor concentrations, considerably exceeding the levels of specific binding to EGFR. Thus, at carefully adjusted concentrations, labeled ML04 is an appropriate tool for measuring EGFR content in cells, displaying adequate levels of specific binding to the target.

### 3.5. Validation of xenograft models by histopathology and immunohistochemistry

Two xenograft models of human glioma cells in nude mice were validated by histopathological and immunohistochemical staining of tumor slices. Several models of U87MG.wt EGFR and U138MG xenografts had been analyzed before an established biologically reproducible model was obtained. Assessed parameters of interest included the following: adequate tumor size to facilitate PET imaging, tumor viability, proliferation, indication of inflammation, blood perfusion and EGFR expression (or lack of it). The most favorable results, obtained with 26-day U87MG.wt EGFR tumors and 14-day U138MG tumors, are presented in Table 2. Both tumor models displayed acceptable proliferation rates and adequate blood perfusion, with few signs of inflammation. The more aggressive phenotype of U138MG cells, clearly detected by an accelerated growth rate of the tumors, could account for both higher percentage of necrosis and fewer blood vessels of these tumors, as compared to U87MG.wt EGFR xenografts. Finally, staining for human EGFR confirmed that overexpression of this target macromolecule was restricted to U87MG.wt EGFR xenografts alone (Fig. 4), endorsing the employment of both tumor models in biodistribution studies.

### 3.6. Biodistribution studies in tumor-bearing nude mice

The in vivo distribution of ML04 in tumor-bearing mice was assessed with the F-18-labeled compound. At first, the

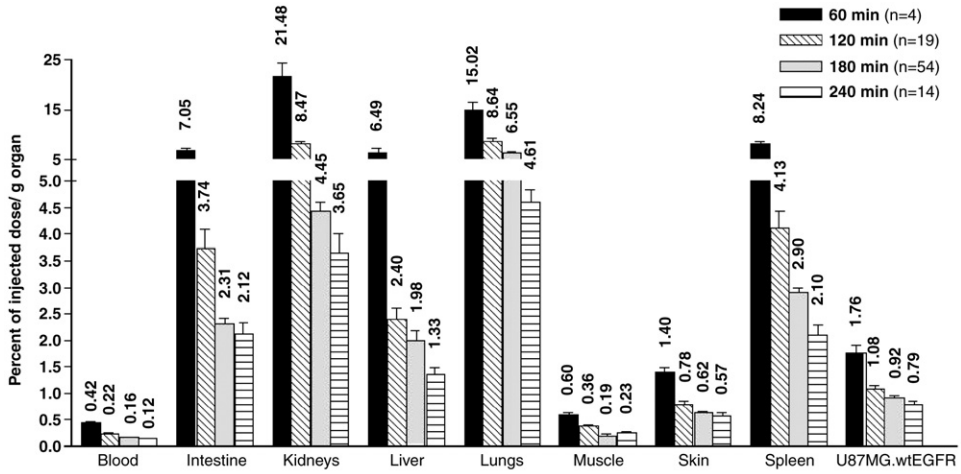


Fig. 5. Distribution of radioactivity at different time points after the injection of **[$^{18}$F]ML04**. Tumor-bearing mice were injected with the labeled compound and sacrificed at various time points after injection of the tracer. Organs were excised and weighed, and their radioactivity content was measured with a γ-counter. Activity uptake is expressed as the mean percentage of injected dose per gram of organ ±S.E.M. Note the break in the *y*-axis to facilitate the comparison of the percentages of injected dose per gram of organ.

Table 3
Effect of vehicle on the biodistribution of **[$^{18}$F]ML04** in U87MG.wt EGFR tumor-bearing mice

| Tissue | % ID/g (mean±S.E.M.) | | Tumor/tissue activity uptake ratio (mean±S.E.M.) | |
|---|---|---|---|---|
| | EtOH/saline ($n$=12) | Intralipid ($n$=37)[a] | EtOH/saline ($n$=10) | Intralipid ($n$=29)[a] |
| Blood | 0.17±0.02 | 0.16±0.01 | 7.07±1.11 | 6.29±0.45 |
| Bone | 0.40±0.05 | 0.40±0.02 | 2.42±0.12 | 2.33±0.13 |
| Heart | 0.33±0.02 | 0.49±0.09 | 3.07±0.20 | 2.28±0.23 |
| Intestine | 2.19±0.14 | 2.31±0.13 | 0.46±0.03 | 0.45±0.02 |
| Kidneys | 3.98±0.25 | 4.57±0.21 | 0.25±0.02 | 0.22±.01 |
| Liver | 1.63±.09 | 2.17±0.28 | 0.59±0.02 | 0.56±0.03 |
| Lungs | 6.11±0.50 | 6.71±0.29 | 0.16±0.01 | 0.14±0.01 |
| Muscle | 0.17±0.03 | 0.20±0.01 | 6.07±0.70 | 4.85±0.33 |
| Skin | 0.59±0.04 | 0.63±0.03 | 1.62±0.05 | 1.49±0.05 |
| Spleen | 2.70±0.19 | 2.96±0.13 | 0.37±0.02 | 0.32±0.01 |
| Stomach | 0.94±0.09 | 1.41±0.13 | 1.13±0.09 | 0.73±0.10 |
| U87MG.wt EGFR tumor | 0.99±0.05 | 0.89±0.04 | | |

Biodistribution studies were carried out 3 h after the administration of **[$^{18}$F]ML04** to U87MG.wt EGFR tumor-bearing mice using either Intralipid 10% or EtOH/saline as vehicle.

[a] The percentages of injected dose per gram of organ of different tissues were obtained from both U87MG.wt EGFR and U138MG tumor-bearing mice, whereas tumor/tissue activity uptake ratios, in particular, were obtained from U87MG.wt EGFR tumor-bearing mice alone.

distribution of radioactivity was assessed at several time points following injection of the tracer (Fig. 5). A rapid decline in radioactivity levels in blood was observed within the first hour, alongside an initial increase and a subsequent decline in radioactivity levels in other examined organs (data not shown). Optimal in vivo imaging quality requires elevated tumor activity concentrations and minimal levels of activity in surrounding tissues to yield good contrast and to facilitate tumor detection. Although activity levels in U87MG.wt EGFR tumors appeared to peak at about 30 min after administration of the tracer, the best tumor/tissue activity uptake ratios were obtained 3 h after injection. Consequently, all comparative studies were carried out at this time point. These were designed to address two issues: (a) comparing Intralipid emulsion with EtOH/saline as vehicle for **[$^{18}$F]ML04**, and (b) demonstrating EGFR-specific uptake of the tracer into the tumor. Thus, the first set of studies was carried out 3 h after the administration of **[$^{18}$F]ML04** in either EtOH/saline or Intralipid. Prior to biodistribution studies with Intralipid, full entrapment of the labeled compound in emulsion drops was confirmed. The results in Table 3, presented both as percentages of injected dose per gram of organ and as tumor/tissue activity uptake ratios, indicate that a more favorable distribution profile was obtained with EtOH/saline as vehicle, albeit no statistically significant differences between the two carriers were revealed. The lungs, kidneys, spleen, small intestine and liver reached the highest activity concentrations of 6.1%, 4.0%, 2.7%, 2.2% and 1.6% ID/g, respectively, compared to ~1% ID/g tumor. Consequently, EtOH/saline was employed as vehicle in subsequent studies.

EGFR-specific tumor uptake of the tracer was assessed by two approaches: (a) employing human glioma EGFR-negative U138MG xenografts as controls, and (b) obstructing EGFR-specific binding by administering excess nonlabeled ML04 prior to the injection of **[$^{18}$F]ML04**. Comparison of the percentages of injected dose per gram of organ obtained for the U138MG and U87MG.wt EGFR tumors revealed higher activity concentrations in EGFR-expressing tumors, which were statistically significant throughout the various time points examined (Fig. 6). However, whereas activity levels of wild-type tumors slowly declined from ~1.1% to ~0.8% ID/g between 120 and 240 min after injection, the measured activity of control tumors remained stable at around 0.65% ID/g. Considering that all other organs demonstrated a decrease in their activity concentrations in this time frame, the invariable levels of activity measured in U138MG tumors were uncharacteristic.

To hamper the binding of the tracer to the receptor, an excess of nonradiolabeled ML04 was administered 1 h before injection of the tracer. Inspection of the data presented in Table 4 reveals essentially higher activity concentrations in the majority of examined tissues in blocking versus control studies, although without statistically significant differences. In contrast, tumor/tissue activity ratios in blocking studies were significantly lower than those in comparative studies, indicating a relatively

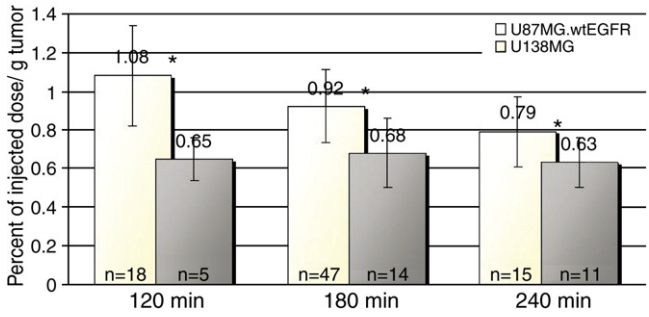


Fig. 6. Preferential uptake of **[$^{18}$F]ML04** in U87MG.wt EGFR over U138MG tumors. Tumor-bearing mice were injected with **[$^{18}$F]ML04** and sacrificed at allotted time points. Tumors were excised, weighed and measured for their radioactivity content with a γ-counter. The percentage of injected dose per gram of tumor was calculated by correcting activity concentration in the tumor for the injected dose. Results are presented as mean±S.D. *Statistically significant differences.

Table 4
Biodistribution of **[$^{18}$F]ML04** in U87MG.wt EGFR tumor-bearing mice with or without preadministration of nonradiolabeled ML04

| Tissue | % ID/g (mean±S.E.M.) | | Tumor/tissue activity uptake ratio (mean±S.E.M.) | |
|---|---|---|---|---|
| | **[$^{18}$F]ML04** ($n$=54)[a] | **[$^{18}$F]ML04** after blocking ($n$=12) | **[$^{18}$F]ML04** ($n$=43)[a] | **[$^{18}$F]ML04** after blocking ($n$=10) |
| Blood | 0.16±0.01 | 0.22±0.02 | 6.97±0.52 | 4.26±0.49 |
| Bone | 0.40±0.02 | 0.49±0.03 | 2.37±0.09 | 1.90±0.15 |
| Heart | 0.43±0.06 | 0.39±0.03 | 2.62±0.17 | 2.27±0.15 |
| Intestine | 2.31±0.10 | 2.79±0.28 | 0.44±0.02 | 0.31±0.03 |
| Kidneys | 4.45±0.16 | 5.24±0.19 | 0.23±0.01 | 0.17±0.01 |
| Liver | 1.98±0.20 | 2.28±0.16 | 0.58±0.02 | 0.38±0.02 |
| Lungs | 6.55±0.23 | 7.25±0.43 | 0.15±0.00 | 0.12±0.01 |
| Muscle | 0.19±0.01 | 0.21±0.01 | 5.11±0.29 | 4.24±0.37 |
| Skin | 0.62±0.02 | 0.62±0.02 | 1.54±0.04 | 1.37±0.05 |
| Spleen | 2.90±0.10 | 3.23±0.15 | 0.33±0.01 | 0.27±0.01 |
| Stomach | 1.23±0.10 | 1.67±0.52 | 0.90±0.08 | 0.87±0.27 |
| U87MG.wt EGFR tumor | 0.92±0.03 | 0.86±0.03 | | |

Biodistribution studies were carried out 3 h after the administration of **[$^{18}$F]ML04** to U87MG.wt EGFR tumor-bearing mice. For blocking studies, unlabeled ML04 was intravenously administered at a dose of 5–8 mg/kg, 60 min before injection of the tracer.

[a] The percentages of injected dose per gram of organ of different tissues were obtained from both U87MG.wt EGFR and U138MG tumor-bearing mice, whereas tumor/tissue activity uptake ratios, in particular, were obtained from U87MG.wt EGFR tumor-bearing mice alone.

lower uptake of activity in tumors compared to that in other tissues after the administration of excess unlabeled ML04.

## 4. Discussion

EGFR is overexpressed in various tumors of epithelial origin, and its overexpression is often associated with poor prognosis, suggestive of its role in the initiation and/or progression of cancer [11]. As a result, several approaches to targeting EGFR in tumors as a means of specific eradication of cancerous cells have been studied. Whether aimed at inhibiting the signaling pathway downstream of this receptor or merely exploiting its overexpression to generate a targeted cytotoxic effect, these approaches require high levels of EGFR expression in tumor cells.

Immunohistochemistry is the method most commonly used to measure the expression level of EGFR in tissue samples, although fluorescence in situ hybridization, ELISA and gene microarrays are employed as alternative methods as well. These techniques tend to be inconsistent and require tumor biopsies, which are not always obtainable. A suitable radiolabeled EGFR-specific agent could establish PET molecular imaging as a noninvasive standard practice to measure EGFR in tumors. Therefore, we investigated the possibility of employing the EGFR tyrosine kinase inhibitor ML04 (Fig. 1) as a bioprobe for PET imaging. Previous reports have demonstrated that derivatives of the 4-dimethylamino-but-2-enoic acid [4-(phenylamino)-quinazoline-6-yl]-amide group are characterized by potent, selective, apparently irreversible inhibition of EGFR. Given its relatively high chemical and biological stabilities, this group of inhibitors was designated for further evaluation, using ML04 as a representative derivative [44].

In the current study, the potency and selectivity of ML04 were further evaluated, using either intact cells or cell-free kinase assays. Prolonged inhibition of EGFR was obtained in various cell lines at low concentrations of ML04 (Table 1). We have not performed measurements that would provide direct evidence of the covalent bonding of the compound to EGFR. Instead, the ability of ML04 to suppress the kinase activity of the receptor in various cell lines 8 h after its removal from the medium and after successive rinsing was demonstrated. Previous reports have used this methodology to support the conception of irreversible binding, using similar chemically structured inhibitors of EGFR (Fig. 7) [44,53–55]. Sustained inhibition of EGFR phosphorylation was attained in those studies following incubation with irreversible compounds, whereas incubation with reversible analogues failed to do so. Furthermore, in the current study, we demonstrated that phosphorylation of EGFR in NCI-H1975 NSCLC cells, which harbor both L858R and T790M mutations in the receptor, was inhibited following incubation with ML04 [59]. T790M mutation confers resistance to reversible EGFR inhibitors, while irreversible inhibitors have been reported to circumvent this resistance [60], thereby providing another indication of covalent bonding between ML04 and EGFR. Finally, molecular modeling studies with a similar derivative of the 4-dimethylamino-but-2-enoic acid [4-(phenylamino)-quinazoline-6-yl]-amide group have been performed, suggesting that the Michael acceptor side chain of this group of inhibitors forms a covalent linkage with EGFR [55]. Altogether, these data strongly support—although do not prove—the irreversible binding of ML04 to EGFR.

The $IC_{50}$ values of ML04 vis-à-vis other investigated tyrosine kinases, namely, PDGFR, VEGFR-2, c-Src and IGF-1 receptor, exceeded those obtained for EGFR by at least two orders of magnitude, revealing adequate levels of selectivity. Nevertheless, the ability of ML04 to distinguish between highly homologous TK domains of EGFR and HER2 was inconclusive, as suggested by comparable $IC_{50}$ values for both tyrosine kinases (Table 1).

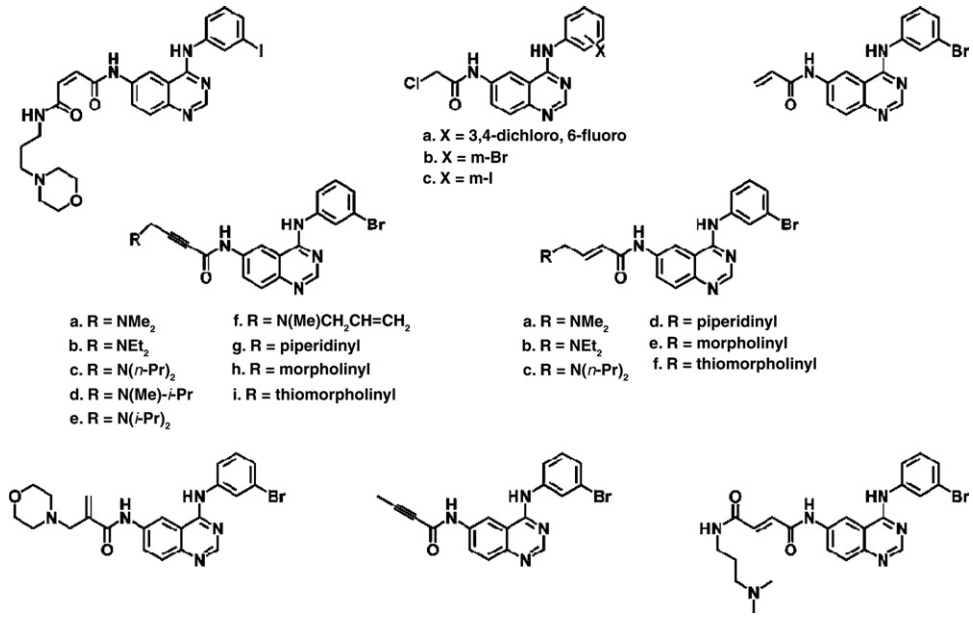


Fig. 7. Selected chemical structures of reported irreversible inhibitors of EGFR [44,53–55,86,87]. Various irreversible inhibitors of EGFR have been introduced in the literature based on the 4-(phenylamino)quinazoline core structure. Commonly, these inhibitors have an attached Michael acceptor functional group at the 6-position of the quinazoline ring. The Michael acceptor side chain of these inhibitors forms a covalent bond with the sulfhydryl group of Cys-773 within the ATP-binding pocket of EGFR.

P-gp is a membranous ATP-dependent efflux pump involved in the multidrug resistance of cancer cells to various chemotherapeutic drugs. It is generally expressed on the apical membrane of cells facing an excretory compartment, such as the gastrointestinal tract, the biliary canalicular front of hepatocytes and biliary ductules, the kidneys and the blood–brain barrier, thereby affecting the disposition of both endogenous molecules and xenobiotics [61,62]. As such, an interaction between P-gp and the labeled compound could, in general, influence the in vivo distribution of the tracer and, in particular, reduce its availability in P-gp-expressing tumors and consequently alter the imaging properties of ML04.

Similar to the chemical structure of ML04, P-gp-interacting compounds are large ($M_W$>300) lipophilic compounds that tend to be cationic at physiological pH and to possess a relatively high number of electron-donating groups (e.g., O, N or groups with a π-electron orbital of an unsaturated system) [62,63]. Moreover, several anilinoquinazoline-based tyrosine kinase inhibitors have been implicated in the inhibition of P-gp and/or other related human transporters [64–66]. Consequently, the interaction between P-gp and ML04 was investigated using human lymphoblastoid CEM Col1000 cells, which express P-gp and control CEM wild-type cells. When compared to the inhibitory effect of verapamil, only 50% inhibition of the transporter was attained at ML04 concentrations of ≥125 μmol/L (data not shown). Conversely, the uptake of [$^{11}$C]ML04 into CEM Col1000 cells almost tripled following the inhibition of P-gp by verapamil (Fig. 2). A similar increase in uptake, caused by the inhibition of the transporter, has been demonstrated both in vitro and in vivo, using typical P-gp substrates such as vinblastine and colchicine [67–70]. Thus, while ML04 does not exert a significant inhibitory effect on P-gp's activity at clinically relevant concentrations, it appears to be subject to the extrusion activity of this transporter.

The development of a reliable imaging agent requires sensitivity of the radioligand to changes in binding site concentration [71]. Therefore, the ability of ML04 to accurately measure the content of EGFR was initially evaluated in vitro with human A431 cells, which express approximately $2\times10^6$ receptors/cell [56–58]. Using the F-18-labeled compound as radiotracer, an accurate measurement of receptor content was obtained, with a maximal specific binding of approximately 75% (Fig. 3). Significant levels of NSB were revealed with increasing inhibitor concentrations. A considerable portion of NSB could also be confirmed by applying an excess of unlabeled ML04 (rather than AG1478) as a competitor in the binding study. If **[$^{18}$F]ML04** did not exclusively bind to EGFR, then addition of the unlabeled compound in excess would result in displacement of the radiotracer from both specific (EGFR) and NSB sites, resulting in overestimation of specific binding. Indeed, the results of this assay (not presented) generated higher derived values of $B_{max}$ ($\approx4\times10^6$ receptors/cell), along with elevated levels of apparent maximal specific binding (87%), confirming a certain affinity of ML04 to macromolecules other than EGFR.

To test the feasibility of employing ML04 as an imaging agent of EGFR-expressing tumors, biodistribution studies were carried out in tumor-bearing nude mice using the F-18-labeled compound. To this end, two xenograft models of subcutaneously injected human glioma cells were established and validated by histopathology and immunohisto-

chemistry. Indicators of viability, proliferation, blood perfusion and inflammation were similar between control (U138MG) and EGFR-positive (U87MG.wt EGFR) tumors, although with an overall slightly better profile of the latter (Table 2). Most importantly, high levels of EGFR expression in U87MG.wt EGFR cells were retained in vivo, whereas U138MG xenografts were devoid of the receptor (Fig. 4), confirming the employment of these tumor models in biodistribution studies. Additionally, since ML04 was found to be a substrate for the extrusion activity of P-gp, the expression of this transporter in both U87MG.wt EGFR and U138MG cell lines was negated.

The kinetics of activity distribution after the injection of **[$^{18}$F]ML04** into tumor-bearing mice designated the 3-h time point as the most favorable one vis-à-vis tumor/tissue activity uptake ratios. At this time, the calculated activity in U87MG.wt EGFR tumors was 0.92% ID/g (25% higher than that in U138MG control tumors), and measured activity in the skin, bone, heart, muscle and blood was 1.5–7 times lower than that in wild-type tumors (Figs. 5 and 6). Higher activity concentrations (twofold to sevenfold) were measured in the lungs, kidneys, spleen small intestine and liver. Those could be accounted for by the presence of EGFR in these murine organs, as well as by their involvement in the excretion and metabolism of drugs [29,72]. As has been previously illustrated, ML04 is a substrate for the efflux mechanism of P-gp and possibly for other physiologically present transport proteins of the ATP-binding cassette superfamily, such as MRP-1. Therefore, high levels of activity uptake in the liver, intestine and kidneys following intravenous administration of **[$^{18}$F]ML04** probably reflect, to some extent, active secretion of the radiotracer or its conjugation derivatives.

Previous reports have indicated that ML04 is more stable in vitro and in vivo than the formerly investigated irreversible EGFR inhibitor ML03, as demonstrated by diminished chemical reactivity of ML04 and higher levels of extraction from blood [42,43]. Hence, whereas the peak tumor/blood activity uptake ratio obtained 1 h after injection of [$^{11}$C]ML03 into tumor-bearing rats merely approached 1, significantly higher ratios were obtained with **[$^{18}$F]ML04** both 1 and 3 h following its administration into nude mice (Fig. 5, Table 4). Nonetheless, to further enhance the relative tumor uptake of **[$^{18}$F]ML04**, the use of an Intralipid 10% emulsion as vehicle was compared to that of an EtOH/saline solution. Previous reports have demonstrated that application of nanoparticulate systems in the delivery of drugs conferred increased in vivo stability of the compounds [73,74]. Nevertheless, current data revealed no advantage of Intralipid over EtOH/saline (Table 3), leading to the employment of an EtOH/saline solution as vehicle in subsequent studies.

Two approaches were undertaken to evaluate EGFR-specific tumor uptake of **[$^{18}$F]ML04**: (a) using EGFR-negative U138MG tumors as controls, and (b) administering an excess of nonlabeled ML04 1 h before injection of the tracer so as to hamper the binding of the tracer to the receptor. As previously pointed out, appreciable activity uptake was observed in U138MG tumors, reaching 60%, 74% and 80% of the total activity uptake in U87MG.wt EGFR tumors at 120, 180 and 240 min after injection, respectively (Fig. 6). While all other examined tissues exhibited a consistent decrease in activity concentrations over time, U138MG tumors were exceptional in their stable levels of activity uptake, yielding increasing control/wild-type tumor activity uptake ratios. The atypical retention of activity observed in control tumors could be accounted for by their relatively more necrotic phenotype, possibly resulting in the presence of a nondisposable blood pool within the tumor. If one were to address bone activity uptake as an indication of defluorination, then steady levels of U138MG activity uptake could also reflect the entrapment of $^{18}$F-labeled fluoride ions in this blood pool.

Blocking studies are often performed to confirm the specific binding of a radiotracer to its target, using an excess of either an identical nonradioactive compound or a structurally different target-specific ligand to occupy the receptor [75–78]. Theoretically, this strategy is likely to reduce the specific uptake of the radioligand, resulting in lower activity concentrations in target tissues. Nevertheless, the administration of unlabeled ML04 in excess 1 h before injection of the tracer resulted in higher activity concentrations in the majority of the organs examined (Table 4). These elevated levels of activity could originate from the inhibition of the elimination processes of the radiotracer following the administration of an excess of ML04, demonstrated by higher blood activity levels in blocking studies as compared to those in control studies. However, to better address this trend, several other aspects should be considered. The general paradigm in the evaluation of potential bioprobes argues that, at high specific activity and when distribution has reached steady state, the binding potential of a radiotracer (indicative of the target/nontarget ratio) is equal to the ratio of the binding site concentration ($B_{max}$) to the equilibrium dissociation constant ($K_d$). Traditionally, a binding potential of $\geq 10$ is considered as a reasonable goal for planar imaging, whereas lower ratios are sufficient for tomography [79,80]. However, it is also well recognized that too large a binding potential might result in transport-dependent distribution, leading to measurement of blood flow rather than of receptor concentration.

Similar to A431 cells, human glioma U87MG.wt EGFR cells express $1\times10^6$ to $3\times10^6$ EGFRs/cell [81]. Assuming $10^9$ cells/g tumor would result in an estimated $B_{max}$ value of 2.5 nmol EGFR/g tumor. Since ML04 is assumed to bind covalently to EGFR, it would be incorrect to refer to its dissociation from the receptor. However, for practical reasons, a very low $K_d$ value could be presumed, thus revealing an extremely high binding potential. It is most likely that, under these conditions, the delivery of **[$^{18}$F]ML04** to U87MG.wt EGFR tumors, rather than binding to EGFR, becomes the rate-limiting step in tumor

uptake since all the delivered radiotracer can be taken up by tumor cells (i.e., tumor uptake of the radioligand reflects blood flow rather than receptor concentration). Therefore, the administration of nonradioactive ML04 in excess in the blocking study in fact raised the input function of the radiotracer, producing higher levels of activity concentration in tissues. In a different blocking study, **[$^{18}$F]ML04** was coadministered with an excess of the EGFR-specific reversible inhibitor AG1478 (2 mg/kg). Still, activity uptake in various tissues was further enhanced compared to earlier blocking studies using unlabeled ML04 (data not shown). Whereas unlabeled ML04 was administered 1 h before injection of the tracer, AG1478 was coinjected with the radiolabeled inhibitor, most likely producing a stronger effect upon delivery of the radiotracer.

It is likely that the flow-limited distribution of **[$^{18}$F]ML04** could be overcome by controlling the input rate of the radiotracer by means of prolonged intravenous infusion. Furthermore, proper chemical modifications in anilinoquinazoline moiety could decelerate the interaction of the inhibitor with EGFR, resulting in lower association constant and reduced binding potential. A similar approach has been applied to [$^{11}$C]L-deprenyl and [$^{11}$C]clorgyline, which are irreversible inhibitors of monoamine oxidase (MAO) B and MAO A, respectively. Both [$^{11}$C]L-deprenyl and [$^{11}$C]clorgyline revealed a robust deuterium isotope effect, whereby substitution of a deuterium atom for a specific hydrogen atom on the methylene carbon of the propagyl group produced significant reduction in the trapping rate of radioligands and enhanced their sensitivities to changes in MAO concentrations [82–84]. Fowler et al. [82,85] have employed this mechanistic tool to image MAO A and MAO B in the human brain, as well as to assess the binding specificity for MAO isoforms in peripheral organs in human subjects. Likewise, minor modifications could be introduced in the chemical structure of ML04, such as the substitution of a deuterium atom for the reactive hydrogen atom at the β-position of the carbonyl. The effect of such alterations in the chemical structure of this radiotracer upon its imaging properties should be further elucidated.

To conclude, ML04 is a selective apparently irreversible inhibitor of EGFR that is capable of accurately measuring EGFR content in cell culture. Biodistribution studies were carried out with human glioma-tumor-bearing mice, using the F-18-labeled compound. Due to higher clearance of activity from nontarget tissues, peak tumor/tissue activity uptake ratios were obtained 3 h after injection, designating this time point for further comparative studies. Despite the remarkable in vitro performance of the inhibitor, only minor EGFR-specific tumor uptake of the labeled compound was demonstrated through blocking studies. Furthermore, significant levels of activity uptake were observed in control EGFR-negative U138MG tumors. Nevertheless, up to 4 h after administration of the radiotracer, the levels of activity uptake in U87MG.wt EGFR tumors were statistically significantly higher than those in control tumors, suggesting that the tumor uptake of the tracer is, at least in part, EGFR-associated. The present results suggest that the distribution of the radiotracer is flow-limited, warranting possible modifications in chemical structure, as well as in the route of administration. Finally, we intend to perform more detailed pharmacokinetic characterization of this bioprobe, which could assist in the development and validation of a kinetic model that would accurately reflect EGFR content in tumors.

## Acknowledgement

Support was provided by TK-Signal Ltd. (Jerusalem, Israel) and Rotem Industries Ltd. (Beer Sheva, Israel).

## References

[1] Hunter T. The epidermal growth factor receptor gene and its product. Nature 1984;311:414–6.
[2] Yarden Y, Schlessinger J. Self-phosphorylation of epidermal growth factor receptor: evidence for a model of intermolecular allosteric activation. Biochemistry 1987;26:1434–42.
[3] Iwashita S, Kobayashi M. Signal transduction system for growth factor receptors associated with tyrosine kinase activity: epidermal growth factor receptor signalling and its regulation. Cell Signal 1992; 4:123–32.
[4] Voldborg BR, Damstrup L, Spang-Thomsen M, Poulsen HS. Epidermal growth factor receptor (EGFR) and EGFR mutations, function and possible role in clinical trials. Ann Oncol 1997;8:1197–206.
[5] Olayioye MA, Neve RM, Lane HA, Hynes NE. The ErbB signaling network: receptor heterodimerization in development and cancer. EMBO J 2000;19:3159–67.
[6] Prenzel N, Fischer OM, Streit S, Hart S, Ullrich A. The epidermal growth factor receptor family as a central element for cellular signal transduction and diversification. Endocr Relat Cancer 2001;8:11–31.
[7] Yarden Y, Sliwkowski MX. Untangling the ErbB signalling network. Nat Rev Mol Cell Biol 2001;2:127–37.
[8] Ritter CA, Arteaga CL. The epidermal growth factor receptor-tyrosine kinase: a promising therapeutic target in solid tumors. Semin Oncol 2003;30:3–11.
[9] Levitzki A. EGF receptor as a therapeutic target. Lung Cancer 2003; 41(Suppl 1):S9–S14.
[10] Stern DF. Tyrosine kinase signalling in breast cancer: ErbB family receptor tyrosine kinases. Breast Cancer Res 2000;2:176–83.
[11] Arteaga CL. Epidermal growth factor receptor dependence in human tumors: more than just expression? Oncologist 2002;7(Suppl 4):31–9.
[12] Fry DW. Protein tyrosine kinases as therapeutic targets in cancer chemotherapy and recent advances in the development of new inhibitors. Expert Opin Investig Drugs 1994;3:577–95.
[13] Mendelsohn J, Baselga J. Status of epidermal growth factor receptor antagonists in the biology and treatment of cancer. J Clin Oncol 2003; 21:2787–99.
[14] http://www.fda.gov/cder/drug/advisory/iressa.htm.
[15] http://www.fda.gov/bbs/topics/news/2004/NEW01139.html.
[16] http://www.fda.gov/bbs/topics/NEWS/2004/NEW01024.html.
[17] Sridhar SS, Seymour L, Shepherd FA. Inhibitors of epidermal-growth-factor receptors: a review of clinical research with a focus on non-small-cell lung cancer. Lancet Oncol 2003;4:397–406.
[18] Bianco R, Daniele G, Ciardiello F, Tortora G. Monoclonal antibodies targeting the epidermal growth factor receptor. Curr Drug Targets 2005;6:275–87.
[19] Adamson ED, Rees AR. Epidermal growth factor receptors. Mol Cell Biochem 1981;34:129–52.

[20] Rachwal W, Bongiorno PF, Orringer MB, Whyte RI, Ethier SP, Beer DG. Expression and activation of erbB-2 and epidermal growth factor receptor in lung adenocarcinomas. Br J Cancer 1995;72:56–64.
[21] Mendelsohn J. The epidermal growth factor receptor as a target for cancer therapy. Endocr Relat Cancer 2001;8:3–9.
[22] Bishop PC, Myers T, Robey R, Fry DW, Liu ET, Blagosklonny MV, et al. Differential sensitivity of cancer cells to inhibitors of the epidermal growth factor receptor family. Oncogene 2002;21:119–27.
[23] Sirotnak FM. Studies with ZD1839 in preclinical models. Semin Oncol 2003;30:12–20.
[24] Arteaga CL, Baselga J. Clinical trial design and end points for epidermal growth factor receptor-targeted therapies: implications for drug development and practice. Clin Cancer Res 2003;9:1579–89.
[25] Gazdar AF, Minna JD. Inhibition of EGFR signaling: all mutations are not created equal. PLoS Med 2005;2:e377.
[26] Sordella R, Bell DW, Haber DA, Settleman J. Gefitinib-sensitizing EGFR mutations in lung cancer activate anti-apoptotic pathways. Science 2004;305:1163–7.
[27] Suzuki T, Nakagawa T, Endo H, Mitsudomi T, Masuda A, Yatabe Y, et al. The sensitivity of lung cancer cell lines to the EGFR-selective tyrosine kinase inhibitor ZD1839 ('Iressa') is not related to the expression of EGFR or HER-2 or to *K-ras* gene status. Lung Cancer 2003;42:35–41.
[28] Lorenzo GD, Bianco R, Tortora G, Ciardiello F. Involvement of growth factor receptors of the epidermal growth factor receptor family in prostate cancer development and progression to androgen independence. Clin Prostate Cancer 2003;2:50–7.
[29] Chen P, Cameron R, Wang J, Vallis KA, Reilly RM. Antitumor effects and normal tissue toxicity of $^{111}$In-labeled epidermal growth factor administered to athymic mice bearing epidermal growth factor receptor-positive human breast cancer xenografts. J Nucl Med 2003; 44:1469–78.
[30] Sundberg AL, Blomquist E, Carlsson J, Steffen AC, Gedda L. Cellular retention of radioactivity and increased radiation dose. Model experiments with EGF-dextran. Nucl Med Biol 2003;30:303–15.
[31] Tolmachev V, Orlova A, Wei Q, Bruskin A, Carlsson J, Gedda L. Comparative biodistribution of potential anti-glioblastoma conjugates [$^{111}$In]DTPA-hEGF and [$^{111}$In]Bz-DTPA-hEGF in normal mice. Cancer Biother Radiopharm 2004;19:491–501.
[32] Mamot C, Drummond DC, Greiser U, Hong K, Kirpotin DB, Marks JD, et al. Epidermal growth factor receptor (EGFR)-targeted immunoliposomes mediate specific and efficient drug delivery to EGFR- and EGFRvIII-overexpressing tumor cells. Cancer Res 2003; 63:3154–61.
[33] Kuan CT, Reist CJ, Foulon CF, Lorimer IA, Archer G, Pegram CN, et al. $^{125}$I-labeled anti-epidermal growth factor receptor-vIII single-chain Fv exhibits specific and high-level targeting of glioma xenografts. Clin Cancer Res 1999;5:1539–49.
[34] Shankar S, Vaidyanathan G, Kuan CT, Binger DD, Zalutsky MR. Antiepidermal growth factor variant III scFv fragment: effect of radioiodination method on tumor targeting and normal tissue clearance. Nucl Med Biol 2006;33:101–10.
[35] Shaul M, Abourbeh G, Jacobson O, Rozen Y, Laky D, Levitzki A, et al. Novel iodine-124 labeled EGFR inhibitors as potential PET agents for molecular imaging in cancer. Bioorg Med Chem 2004;12:3421–9.
[36] Noonberg SB, Benz CC. Tyrosine kinase inhibitors targeted to the epidermal growth factor receptor subfamily: role as anticancer agents. Drugs 2000;59:753–67.
[37] Fredriksson A, Johnstrom P, Thorell JO, von Heijne G, Hassan M, Eksborg S, et al. In vivo evaluation of the biodistribution of $^{11}$C-labeled PD153035 in rats without and with neuroblastoma implants. Life Sci 1999;65:165–74.
[38] Seimbille Y, Phelps ME, Czernin J, Silverman DHS. Fluorine-18 labeling of 6,7-disubstituted anilinoquinazoline derivatives for positron emission tomography (PET) imaging of tyrosine kinase receptors: synthesis of $^{18}$F-Iressa and related molecular probes. J Labelled Compd Radiopharm 2005;48:829–43.
[39] Vasdev N, Dorff PN, Gibbs AR, Nandanan E, Reid LM, O'Neil JP, et al. Synthesis of 6-acrylamido-4-(2-[$^{18}$F]fluoroanilino)quinazoline: a prospective irreversible EGFR binding probe. J Labelled Compd Radiopharm 2005;48:109–15.
[40] VanBrocklin HF, Lim JK, Coffing SL, Hom DL, Negash K, Ono MY, et al. Anilinodialkoxyquinazolines: screening epidermal growth factor receptor tyrosine kinase inhibitors for potential tumor imaging probes. J Med Chem 2005;48:7445–56.
[41] Mishani E, Abourbeh G, Rozen Y, Jacobson O, Laky D, Ben David I, et al. Novel carbon-11 labeled 4-dimethylamino-but-2-enoic acid [4-(phenylamino)-quinazoline-6-yl]-amides: potential PET bioprobes for molecular imaging of EGFR-positive tumors. Nucl Med Biol 2004;31: 469–76.
[42] Bonasera TA, Ortu G, Rozen Y, Krais R, Freedman NM, Chisin R, et al. Potential (18)F-labeled biomarkers for epidermal growth factor receptor tyrosine kinase. Nucl Med Biol 2001;28:359–74.
[43] Ortu G, Ben-David I, Rozen Y, Freedman NM, Chisin R, Levitzki A, et al. Labeled EGFR-TK irreversible inhibitor (ML03): in vitro and in vivo properties, potential as PET biomarker for cancer and feasibility as anticancer drug. Int J Cancer 2002;101:360–70.
[44] Mishani E, Abourbeh G, Jacobson O, Dissoki S, Ben Daniel R, Rozen Y, et al. High-affinity epidermal growth factor receptor (EGFR) irreversible inhibitors with diminished chemical reactivities as positron emission tomography (PET)-imaging agent candidates of EGFR overexpressing tumors. J Med Chem 2005;48:5337–48.
[45] Gazit A, Chen J, App H, McMahon G, Hirth P, Chen I, et al. Tyrphostins IV — highly potent inhibitors of EGF receptor kinase. Structure–activity relationship study of 4-anilidoquinazolines. Bioorg Med Chem 1996;4:1203–7.
[46] Huang HS, Nagane M, Klingbeil CK, Lin H, Nishikawa R, Ji XD, et al. The enhanced tumorigenic activity of a mutant epidermal growth factor receptor common in human cancers is mediated by threshold levels of constitutive tyrosine phosphorylation and unattenuated signaling. J Biol Chem 1997;272:2927–35.
[47] Karni R, Mizrachi S, Reiss-Sklan E, Gazit A, Livnah O, Levitzki A. The pp60c-Src inhibitor PP1 is non-competitive against ATP. FEBS Lett 2003;537:47–52.
[48] Blum G, Gazit A, Levitzki A. Substrate competitive inhibitors of IGF-1 receptor kinase. Biochemistry 2000;39:15705–12.
[49] Kohler S, Stein WD. Optimizing chemotherapy by measuring reversal of P-glycoprotein activity in plasma membrane vesicles. Biotechnol Bioeng 2003;81:507–17.
[50] Krishna R, Mayer LD. Modulation of P-glycoprotein (PGP) mediated multidrug resistance (MDR) using chemosensitizers: recent advances in the design of selective MDR modulators. Curr Med Chem Anti-Canc Agents 2001;1:163–74.
[51] Stein WD. Reversers of the multidrug resistance transporter P-glycoprotein. Curr Opin Investig Drugs 2002;3:812–7.
[52] Dissoki S, Laky D, Mishani E. Fluorine-18 labeling of ML04 — presently the most promising irreversible inhibitor candidate for visualization of EGFR in cancer. J Labelled Compd Radiopharm 2006;49:533–43.
[53] Fry DW, Bridges AJ, Denny WA, Doherty A, Greis KD, Hicks JL, et al. Specific, irreversible inactivation of the epidermal growth factor receptor and erbB2, by a new class of tyrosine kinase inhibitor. Proc Natl Acad Sci U S A 1998;95:12022–7.
[54] Smaill JB, Showalter HD, Zhou H, Bridges AJ, McNamara DJ, Fry DW, et al. Tyrosine kinase inhibitors: 18. 6-Substituted 4-anilinoquinazolines and 4-anilinopyrido[3,4-*d*]pyrimidines as soluble, irreversible inhibitors of the epidermal growth factor receptor. J Med Chem 2001;44:429–40.
[55] Tsou HR, Mamuya N, Johnson BD, Reich MF, Gruber BC, Ye F, et al. 6-Substituted-4-(3-bromophenylamino)quinazolines as putative irreversible inhibitors of the epidermal growth factor receptor (EGFR) and human epidermal growth factor receptor (HER-2) tyrosine kinases with enhanced antitumor activity. J Med Chem 2001;44: 2719–34.

[56] Krupp MN, Connolly DT, Lane MD. Synthesis, turnover, and down-regulation of epidermal growth factor receptors in human A431 epidermoid carcinoma cells and skin fibroblasts. J Biol Chem 1982; 257:11489–96.

[57] Haigler H, Ash JF, Singer SJ, Cohen S. Visualization by fluorescence of the binding and internalization of epidermal growth factor in human carcinoma cells A-431. Proc Natl Acad Sci U S A 1978;75:3317–21.

[58] Goldenberg A, Masui H, Divgi C, Kamrath H, Pentlow K, Mendelsohn J. Imaging of human tumor xenografts with an indium-111-labeled anti-epidermal growth factor receptor monoclonal antibody. J Natl Cancer Inst 1989;81:1616–25.

[59] Pao W, Miller VA, Politi KA, Riely GJ, Somwar R, Zakowski MF, et al. Acquired resistance of lung adenocarcinomas to gefitinib or erlotinib is associated with a second mutation in the EGFR kinase domain. PLoS Med 2005;2:e73.

[60] Kwak EL, Sordella R, Bell DW, Godin-Heymann N, Okimoto RA, Brannigan BW, et al. Irreversible inhibitors of the EGF receptor may circumvent acquired resistance to gefitinib. Proc Natl Acad Sci U S A 2005;102:7665–70.

[61] Thiebaut F, Tsuruo T, Hamada H, Gottesman MM, Pastan I, Willingham MC. Cellular localization of the multidrug-resistance gene product P-glycoprotein in normal human tissues. Proc Natl Acad Sci U S A 1987;84:7735–8.

[62] Ambudkar SV, Dey S, Hrycyna CA, Ramachandra M, Pastan I, Gottesman MM. Biochemical, cellular, and pharmacological aspects of the multidrug transporter. Annu Rev Pharmacol Toxicol 1999;39: 361–98.

[63] Matheny CJ, Lamb MW, Brouwer KR, Pollack GM. Pharmacokinetic and pharmacodynamic implications of P-glycoprotein modulation. Pharmacotherapy 2001;21:778–96.

[64] Hegedus T, Orfi L, Seprodi A, Varadi A, Sarkadi B, Keri G. Interaction of tyrosine kinase inhibitors with the human multidrug transporter proteins, MDR1 and MRP1. Biochim Biophys Acta 2002; 1587:318–25.

[65] Elkind NB, Szentpetery Z, Apati A, Ozvegy-Laczka C, Varady G, Ujhelly O, et al. Multidrug transporter ABCG2 prevents tumor cell death induced by the epidermal growth factor receptor inhibitor Iressa (ZD1839, gefitinib). Cancer Res 2005;65:1770–7.

[66] Kitazaki T, Oka M, Nakamura Y, Tsurutani J, Doi S, Yasunaga M, et al. Gefitinib, an EGFR tyrosine kinase inhibitor, directly inhibits the function of P-glycoprotein in multidrug resistant cancer cells. Lung Cancer 2005;49:337–43.

[67] Zacherl J, Hamilton G, Thalhammer T, Riegler M, Cosentini EP, Ellinger A, et al. Inhibition of P-glycoprotein-mediated vinblastine transport across HCT-8 intestinal carcinoma monolayers by verapamil, cyclosporine A and SDZ PSC 833 in dependence on extracellular pH. Cancer Chemother Pharmacol 1994;34:125–32.

[68] Mehta BM, Rosa E, Fissekis JD, Bading JR, Biedler JL, Larson SM. In-vivo identification of tumor multidrug resistance with $^{3}$H-colchicine [corrected]. J Nucl Med 1992;33:1373–7.

[69] Achira M, Suzuki H, Ito K, Sugiyama Y. Comparative studies to determine the selective inhibitors for P-glycoprotein and cytochrome *P*4503A4. AAPS PharmSci 1999;1:E18.

[70] Horio M, Pastan I, Gottesman MM, Handler JS. Transepithelial transport of vinblastine by kidney-derived cell lines. Application of a new kinetic model to estimate in situ $K_m$ of the pump. Biochim Biophys Acta 1990;1027:116–22.

[71] Eckelman WC. The status of radiopharmaceutical research. Int J Rad Appl Instrum B 1991;18:iii–vi.

[72] Mateo de Acosta C, Justiz E, Skoog L, Lage A. Biodistribution of radioactive epidermal growth factor in normal and tumor bearing mice. Anticancer Res 1989;9:87–92.

[73] Majeti N, Ravi K. Nano and microparticles as controlled drug delivery devices. J Pharm Pharm Sci 2000;3:234–58.

[74] Fishbein I, Chorny M, Rabinovich L, Banai S, Gati I, Golomb G. Nanoparticulate delivery system of a tyrphostin for the treatment of restenosis. J Control Release 2000;65:221–9.

[75] Katzenellenbogen JA, Mathias CJ, VanBrocklin HF, Brodack JW, Welch MJ. Titration of the in vivo uptake of 16 alpha-[$^{18}$F]fluoroestradiol by target tissues in the rat: competition by tamoxifen, and implications for quantitating estrogen receptors in vivo and the use of animal models in receptor-binding radiopharmaceutical development. Nucl Med Biol 1993;20:735–45.

[76] Gildersleeve DL, Lin TY, Wieland DM, Ciliax BJ, Olson JM, Young AB. Synthesis of a high specific activity $^{125}$I-labeled analog of PK 11195, potential agent for SPECT imaging of the peripheral benzodiazepine binding site. Int J Rad Appl Instrum B 1989;16: 423–9.

[77] Gibson RE, Beauchamp HT, Fioravanti C, Brenner N, Burns HD. Receptor binding radiotracers for the angiotensin II receptor: radioiodinated [Sar$_1$, Ile$_8$] angiotensin II. Nucl Med Biol 1994;21: 593–600.

[78] Bakker WH, Krenning EP, Reubi JC, Breeman WA, Setyono-Han B, de Jong M, et al. In vivo application of [$^{111}$In-DTPA-D-Phe$_1$]-octreotide for detection of somatostatin receptor-positive tumors in rats. Life Sci 1991;49:1593–601.

[79] Eckelman WC. Sensitivity of new radiopharmaceuticals. Nucl Med Biol 1998;25:169–73.

[80] Eckelman WC. The application of receptor theory to receptor-binding and enzyme-binding oncologic radiopharmaceuticals. Nucl Med Biol 1994;21:759–69.

[81] Nishikawa R, Ji XD, Harmon RC, Lazar CS, Gill GN, Cavenee WK, et al. A mutant epidermal growth factor receptor common in human glioma confers enhanced tumorigenicity. Proc Natl Acad Sci U S A 1994;91:7727–31.

[82] Fowler JS, Logan J, Wang GJ, Volkow ND, Telang F, Zhu W, et al. Low monoamine oxidase B in peripheral organs in smokers. Proc Natl Acad Sci U S A 2003;100:11600–5.

[83] Fowler JS, Wang GJ, Logan J, Xie S, Volkow ND, MacGregor RR, et al. Selective reduction of radiotracer trapping by deuterium substitution: comparison of carbon-11-L-deprenyl and carbon-11-deprenyl-$D_2$ for MAO B mapping. J Nucl Med 1995;36:1255–62.

[84] Logan J, Fowler JS, Volkow ND, Wang GJ, MacGregor RR, Shea C. Reproducibility of repeated measures of deuterium substituted [$^{11}$C]L-deprenyl ([$^{11}$C]L-deprenyl-$D_2$) binding in the human brain. Nucl Med Biol 2000;27:43–9.

[85] Fowler JS, Logan J, Volkow ND, Wang GJ. Translational neuroimaging: positron emission tomography studies of monoamine oxidase. Mol Imaging Biol 2005;7:377–87.

[86] Pal A, Glekas A, Doubrovin M, Balatoni J, Beresten T, Maxwell D, et al. Molecular imaging of EGFR kinase activity in tumors with (124)I-labeled small molecular tracer and positron emission tomography. Mol Imaging Biol 2006;8:262–77.

[87] Discafani CM, Carroll ML, Floyd Jr MB, Hollander IJ, Husain Z, Johnson BD, et al. Irreversible inhibition of epidermal growth factor receptor tyrosine kinase with in vivo activity by *N*-[4-[(3-bromophenyl)amino]-6-quinazolinyl]-2-butynamide (CL-387,785). Biochem Pharmacol 1999;57:917–25.